Helium Ion Microscopy for Reduced Spin Orbit Torque Switching Currents

Dunne, P.; Fowley, C.; Hlawacek, G.; Kurian, J.; Atcheson, G.; Colis, S.; Teichert, N.; Kundys, B.; Venkatesan, M.; Lindner, J.; Deac, A. M.; Hermans, T.; Coey, J.; Doudin, B.;

Originally published:

September 2020

Nano Letters 20(2020)10, 7036-7042

DOI: https://doi.org/10.1021/acs.nanolett.0c02060

Helium Ion Microscopy for Reduced Spin Orbit Torque Switching Currents

Peter Dunne[1,2‡], Ciaran Fowley[3*‡], Gregor Hlawacek[3], Jinu Kurian[1], Gwenaël Atcheson[4], Silviu Colis[1], Niclas. Teichert[4], Bohdan Kundys[1], M Venkatesan[4], Jürgen Lindner[3], Alina Maria Deac[3], Thomas M. Hermans[2], J. Mike D. Coey[4], Bernard Doudin[1]*

[1]Université de Strasbourg, CNRS, IPCMS UMR 7504, 23 rue du Loess, F-67034 Strasbourg, France

[2]Université de Strasbourg, CNRS, ISIS, 8 allée Gaspard Monge, 67000 Strasbourg, France

[3]Institute of Ion Beam Physics and Materials Research, Helmholtz-Zentrum Dresden - Rossendorf, Bautzner Landstraße 400, 01328 Dresden, Germany

[4]AMBER and School of Physics, Trinity College, Dublin 2, Ireland

KEYWORDS spintronics, spin orbit torque switching, nanomagnetism, ion beam irradiation

ABSTRACT

Spin orbit torque driven switching is a favourable way to manipulate nanoscale magnetic objects for both memory and wireless communication devices. The critical current required to switch from one stored magnetic state to another depends on the multilayer structure of the device and the intrinsic properties of the materials used, which are difficult to control on a local scale. Here we demonstrate how focused helium ion beam irradiation can be used to modulate the local magnetic anisotropy of a Co thin film at the microscopic scale. *In-situ* characterisation using the anomalous Hall effect showed up to an order of magnitude reduction of the magnetic anisotropy under irradiation in real-time, and using this, a multi-level storage element is demonstrated. The result is that current-driven spin-switching, with as little as 800 kA cm^{-2} can be achieved on predetermined areas of the film without the need for physical material patterning.

MAIN TEXT

Spin transport across material interfaces is sensitive to the electronic and structural nature of the interface. Since the discovery of giant magnetoresistance in the late 1980's[1,2] through to the theoretical[3] and experimental realisation of spin transfer torque[4,5], the field of spintronics has grown steadily, with modern data storage already exploiting conventional spin transfer torque to change magnetisation states in magnetic tunnel junctions[6]. Spin orbit torque (SOT) switching, on the other hand, is a relatively young field[7–9], relying on the spin Hall[9] and Rashba[10] effects to manipulate static and dynamic magnetisation states by the flow of electrical current in adjacent heavy metal (HM) layers. In contrast to spin-transfer-torque MRAMs[11], SOT devices require less demanding 3D fabrication, greatly simplifying their production. Moreover, their planar nature

allows for easy visualisation and easier exploitation of the stray magnetic fields in applications such as reprogrammable magnetic domain configurations for spin-wave logic[12].

The present drive to reduce switching currents and energy consumption is constrained by the selection of materials necessary to switch a magnetic domain *via* SOT. Similarly, real devices require multi-step nanofabrication to define memory storage cells. Here we present a new method to both reduce the switching currents, and to avoid multi-step lithography by using He^+ irradiation to locally modify the material properties in a single layer. Consequently, we can reduce the critical current density in a macroscopic device by almost an order of magnitude. Furthermore, we demonstrate how *in-situ* electrical measurement during irradiation allows precise control over the manipulation of the perpendicular magnetic anisotropy, capturing its evolution as a function of ion dose, making possible high-precision control and reproducibility of the process.

Light ion irradiation can lead to structural reorganization of stable material phases while preserving overall atomic composition with little to no topological damage[13]. This allows for the reduction of PMA in thin magnetic multilayers[14,15], which is caused by the intermixing of layers and increase of interfacial roughness[13]. Furthermore, He^+ and Ar^+ broad-beam irradiation has been used to tailor SOT driven domain-wall dynamics[16], improve the spectral linewidth of SOT nano-oscillators[17], and reduce the critical current density to switch the magnetisation of extended thin films via SOT[18]. Patterned magnetic anisotropy using broad beam irradiation has been demonstrated using shadow masks, but the smallest patterned volumes are mostly determined by the lithography process rather than the ion-beam interaction volume.[15] On the contrary, focused helium ion beams allow precise control of perpendicular magnetic anisotropy[19,20] and magnetisation[21] on the order of the diameter of the ion beam (< 2 nm)[22].

Samples of Ta(5)/Pt(2)/Co(1.0)/W(1.5)/Pt(1.5)/Ta(1.5) were prepared by magnetron sputtering on Si wafers, and patterned into 10 μm Hall bar structures by a combination of UV lithography, ion milling and lift-off. An asymmetric stack of Pt, Co, and W was chosen, as the opposite spin Hall angles of the Pt-Co and Co-W interfaces is known to maximise SOT switching efficiency[23]. SQUID magnetometry on unpatterned films with the substrate orientated parallel and perpendicular to the applied field indicated robust PMA (Fig. 1a), as expected for a sub-nm Co film[24], with an effective anisotropy field of 1.28 T, and a saturation magnetisation $\mu_0 M_s$ of 1.02 T. Anomalous Hall effect measurements confirmed that the PMA remains intact on the patterned Hall bars (Figs. 1b,c). Here, we found square hysteresis loops and coercivities of ~20 mT (Fig. 1b) for magnetic fields applied perpendicular to the film along z, and effective magnetic anisotropies of well over 1 T (Fig. 1c) for hard axis measurements (along x). At positive saturation ($+m_z$), the anomalous Hall resistance is 0.59 Ω.

Current-induced (I_x) switching measurements under a bias field $\mu_0 H_x$ = 150 mT (Fig 1d) yield a critical current density, J_c, of 6.0 MA/cm² for full magnetisation reversal in the microfabricated structure. To minimise thermal effects while sweeping the current, I_x was pulsed for a duration of 2 ms, with a delay of 1 s between subsequent pulses, i.e., a duty cycle of 0.2%. Similar to the field driven switching in Fig. 1b, there is only one step and the saturated state has a resistance of 0.57 Ω.

The patterned devices were locally irradiated with helium ions with a 30 kV acceleration voltage using an Orion Nanofab+ helium ion microscope system, while in real time, we monitored the evolution of the anomalous Hall resistance *in-situ*. This electrical characterisation system consists of four Kleindieck MM3A micromanipulators which allow three-dimensional positioning of the contacting needles in a high vacuum environment (see Fig. 2a). A Keithley

2400 source meter was used to apply current and read the voltage drop corresponding to the longitudinal and transverse resistances. A current of 1 mA applied along the *x*-axis is used to probe the evolution of the anomalous Hall resistance close to zero applied magnetic field.

During irradiation, the anomalous Hall resistance steadily decreases (Fig. 2b) until a critical dose of 35 ions/nm² is reached, and a sharp switching is observed. The sharp fall in ΔR is complete at 37 ions/nm². The total fall of resistance (0.52 Ω) is close to the full deflection observed in the *ex-situ* measurements shown in Fig. 1, marked as a grey dashed line, and indicates a reduced effective anisotropy field in the irradiated zone (H_{K2}) compared to that of the extended structure (H_{K1}) (Fig. 2b). The layer intermixing introduced by irradiation gives control over K_{eff}, and H_{K2} thus becomes an experimentally tuneable parameter. Although the irradiations were carried out over the complete area of the Hall cross, as shown in Fig. 2c, the close proximity of the unirradiated areas allow for residual information from those regions to be gathered in the Hall loops, leading to the offset of ~0.1 Ω in Fig. 2b.

We selected four doses along this irradiation curve to demonstrate the ease of applying this technique to the reduction of critical currents for spin orbit torque switching. Figure 2d shows the corresponding anomalous Hall response versus $\mu_0 H_x$. for 1, 20, 30, and 50 ions/nm². Aside from the reduction in magnetic anisotropy field, evidenced by the saturation of R_{AHE} at lower in-plane applied fields, several steps are observed in the anomalous Hall loops for irradiation doses ≥30 ions/nm^2. The additional steps correspond to the unchanged anisotropy in the unirradiated adjacent regions. This offset is highly dependent on the accuracy of overlaying the irradiation box with the junction area, and the residual Hall resistance is never precisely the same for each junction. However, the multi-step switching, as seen in Fig, 2d, is always a result of the reversal of neighbouring regions adjoint the Hall cross.

Assuming coherent rotation of the magnetisation, the normalised first quadrant magnetisation, $M_z^{'}$, (Fig. 2e) can be fitted with[25]

$$M_z^{'}=\sqrt{1-\left(\frac{\mu_0 H_x}{\mu_0 H_K}\right)^2} \quad (1)$$

which yields the magnetic anisotropy field, $\mu_0 H_K$, as a function of irradiation dose (Fig. 2f). We observe a continuous decrease in the anisotropy field, from 1.32 T for as-deposited films, to as small as 0.12 T for samples irradiated beyond the critical dose of 35 ions/nm^2. The saturation magnetisation, M_s, (Fig. 2f) was determined from the relative change in the saturation Hall resistance with ion dose. M_s is reduced at higher ion doses, due to alloying of the Co/HM interfaces, but is less sensitive than the magnetic anisotropy field, H_K, only reducing to 86% of the initial value compared to 33% for the anisotropy field after a dose of 30 ions/nm^2.

Both the H_K and M_s play an important role in current-induced SOT switching. Under a macrospin approximation with the condition $H_x \ll H_K$, where H_x is a magnetic bias field applied in-plane, the critical current density, J_c, required to switch the magnetisation direction of a magnetic state (in SI units) is[26]

$$J_c=\frac{2e\mu_0 M_s t_f}{\hbar\,\theta_{SH}}\left(\frac{H_K}{2}-\frac{H_x}{\sqrt{2}}\right) \quad (2)$$

where e is the electronic charge, $\hbar$ is the reduced Planck constant, t_f is the magnetic free-layer thickness, and θ_{SH} is the spin Hall angle. However, when the applied field is comparable to the anisotropy, as we find for increased ion doses, the critical current density can instead be written as[26]

$$J_c = \frac{2e\mu_0 M_s t_f}{\hbar\,\theta_{SH}}\left(\sqrt{\frac{H_K^2}{32}\left[8+20b^2-b^4-b\left(8+b^2\right)^{3/2}\right]}\right) \quad (3)$$

where $b = H_x / H_K$. The effect of ion dose on J_c is initially minimal for doses up to 20 ions/nm^2 (Figs. 2f, 3a, & Table 1), with J_c^{-+} reducing from -6.0 to -5.0 MA cm^{-2} (for $\mu_0 H_x$ = 150 mT). For 30 ions/nm^2, close to the critical dose, the critical current density is, however, reduced by almost one order of magnitude to -800 kA cm^{-2}. At larger doses, 50 ions nm^{-2}, we only observe the switching in the peripheral regions adjacent to the Hall cross.

Nonetheless, reducing the critical current density is not the sole criterion for improvement of SOT switching of magnet states. Additionally, we define a SOT switching efficiency, being the ratio of the magnetic energy barrier (K_U) per unit area (in the magnetic free layer t_f) versus the electrical power (P) per unit area (in the entire stack thickness, d) required to switch the magnetic state, in units of seconds:

$$\eta = \frac{K_U t_f}{Pd} = \frac{\mu_0 M_s \left(H_K - H_x\right) t_f}{2 J_c^2 \rho d} \quad (4)$$

where ρ is the total resistivity of the device. Defined in this way, the switching efficiency of different material systems can be compared, so long as the bias fields are similar. If this is not the case, substituting J_c from eq. (2) into (4) under the condition $H_x \ll H_K$, leads to an intrinsic SOT efficiency for PMA systems:

$$\eta_i = \frac{\hbar^2 \theta_{SH}^2}{2\mu_0 M_s H_K e^2 \rho d\, t_f} \quad (5)$$

The advantage of eq. (4) is that it depends solely on intrinsic material properties, and not on the experimental conditions, thus making it a more transparent comparator between different

reported systems. Its drawback is that it is based on a macrospin approximation, which cannot consider a multidomain response, and overestimates the critical current density by a factor 10 - 100.

Nevertheless, this expression illustrates that to achieve large switching efficiencies, a minimal amount of conductive material must be used, while retaining a large spin Hall angle and a small anisotropy field. Similar to J_c, we find there is negligible change in the intrinsic switching efficiency, η_i, for irradiation doses < 20 ion nm^{-2}, which remains close to 15 fs (Table 1), increases to a maximum of 53 fs at 30 ions nm^{-2}. In contrast the experimental efficiency, η, is initially ~110 ps, and *drops* at 20 ions nm^{-2} to 68 ps, before then increasing to its maximum of 1382 at 30 ions nm^{-2}, an order of magnitude improvement upon the virgin state. In all cases, the switching efficiency compares favourably to the literature (listed in Table 2), which have efficiencies typically of order 0.1 - 10 ps, with a maximum of 201 ps found for insulating barium ferrite on Pt[27], and 106 ps for metallic Pt/Co/Cr/Ta multilayers[28].

Returning to the SOT switching for 30 ions/nm², shown in Fig. 3a, we sketch the magnetic states at points 1, 2, 3 and 4 in Fig. 3b. As the interior of the Hall cross can be addressed separately to the rest of device, this forms a two-state system that can be addressed electrically as shown in Fig. 3a, or magnetically as shown in Figs. 2c and 3c,d. Electrical switching involves applying a bias in-plane field (here 150 mT), and pulsing currents in a range of ± 3 mA to ensure switching of only the irradiated region. This leads to a switch between states 1 and 2, or 3 and 4 in (Fig. 3a,b). Otherwise pulsing currents of order ± 7.5 mA switches the magnetisation of the entire device between states 1 and 3 (Fig. 3a,b). Magneto-optic Kerr effect (MOKE) imaging under magnetic fields normal to the device ($\mu_0 H_z$) confirms that the entire irradiated region switches independently from the rest of the device, Fig. 3c. Individual

hysteresis loops for the irradiated (30 ions nm^{-2}) and nonirradiated regions (as-dep_1, as-dep_2) are shown in Fig. 3d. The irradiated and unirradiated regions exhibit coercivities which are well spaced in magnetic field, $\mu_0 H_c$ = 5 mT and $\mu_0 H_c$ = 16 mT, respectively. The reader is directed to the supplementary video 1 to view the full magnetisation response during a field sweep.

Although there is an equivalence between electrical and magnetic switching, electrical SOT switching is more robust to variability in lithographic processing of the Hall bars than magnetic switching. This is because the former depends on the perpendicular magnetic anisotropy of a device, compared to coercivity for the latter. We find less than 1% variation in the magnetic anisotropy for the non-irradiated devices, $\mu_0 H_K$ =1.32 ± 0.01 T, as the anisotropy is determined by the deposition process, which in bulk, non-patterned, thin films is 1.28 ± 0.05 T. In contrast, we find a 26% variation of coercivity in the same devices, 14 ± 4 mT, reflecting the strong dependence of the coercivity on the lithographic processing and slight variations in dimensions of the Hall bars. Since we address the anisotropy directly with ion irradiation, this illustrates the advantageous precision and robustness of focussed ion beam irradiation for magnetic element patterning compared to material removal.

In order to assess the suitability of the device as a memory storage element, we analyse the effect of He^+ irradiation on the thermal stability of the created magnetic bits. As expected, the reduction in J_c does come at the cost of thermal stability, $\Delta = K_{eff} V / k_B T$, where V is the magnetic element volume k_B is Boltzmann's constant and T is temperature. However, even for a 1 nm thick, 32 nm sided element, i.e. a 1024 nm^3 volume, Δ = 64 for doses as high as 20 ions nm^{-2}, more than the 10-year stability criterion of 60 used in magnetic recording[29]. Close to the critical dose, at 30 ions nm^{-2}, Δ drops to 38—the equivalent of 95% data retention for 16 days[30]—but unlike data storage, long-term stability is not critical to all applications. In fact, weakly bi-

stable devices can be suitable for spin Hall oscillators, where the strength and modulation of spin wave propagation depends on the magnetic anisotropy[31]. Furthermore, the reduction in local magnetic anisotropy allows for minimal losses during magnetisation switching. This level of control highlights the effectiveness of this method to tailor the switching current density in PMA multilayers.

In summary, a He^+ microscope has been used to perform mask-less light-ion irradiation on perpendicular magnetic anisotropy stacks for local control of the SOT switching properties. *In-situ* electrical measurements of anisotropy reduction provides real-time control of the anisotropy, allowing accurate determination of the critical dose needed to reach a desired value of the anisotropy, up to the transition to in-plane magnetic anisotropy. The corresponding reduction in critical current densities for SOT switching are nearly linear with decreasing anisotropy. Irradiation at doses just below the critical dose allow us to achieve almost an order of magnitude control over the critical current required for robust switching, and DC switching current densities as low as 800 kA cm^{-2} are achieved, which we believe is the lowest to date. Moreover, the switching efficiency of 1381 ps is an order of magnitude larger than previous state of the art. It illustrates the unique advantages of this approach, and opens the door to preferential switching of predetermined areas of the sample, limited by the nm-resolution of the He^+ ion beam microscopy, while preserving the flat topography of the initial magnetic stack.

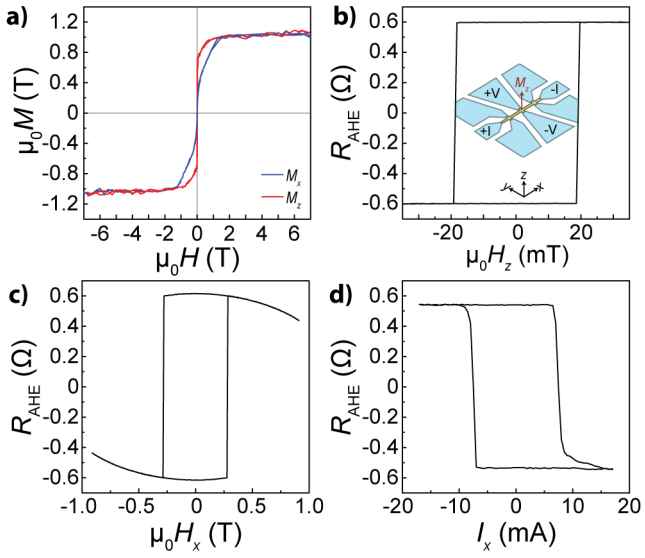
a)
b)
c)
d)
$\mu_0 M$ (T)
$\mu_0 H$ (T)
M_x
M_z
R_{AHE} (Ω)
$\mu_0 H_z$ (mT)
+V
-I
+I
-V
M_z
z
$\mu_0 H_x$ (T)
I_x (mA)

Figure 1. a) SQUID-VSM magnetometry parallel (M_x) and perpendicular (M_z) to the substrate. The anomalous Hall resistance of virgin junctions versus **b)** $\mu_0 H_z$; **c)** $\mu_0 H_x$; and **d)** applied DC pulse current, I_x, under a bias field of $\mu_0 H_x = 150$ mT.

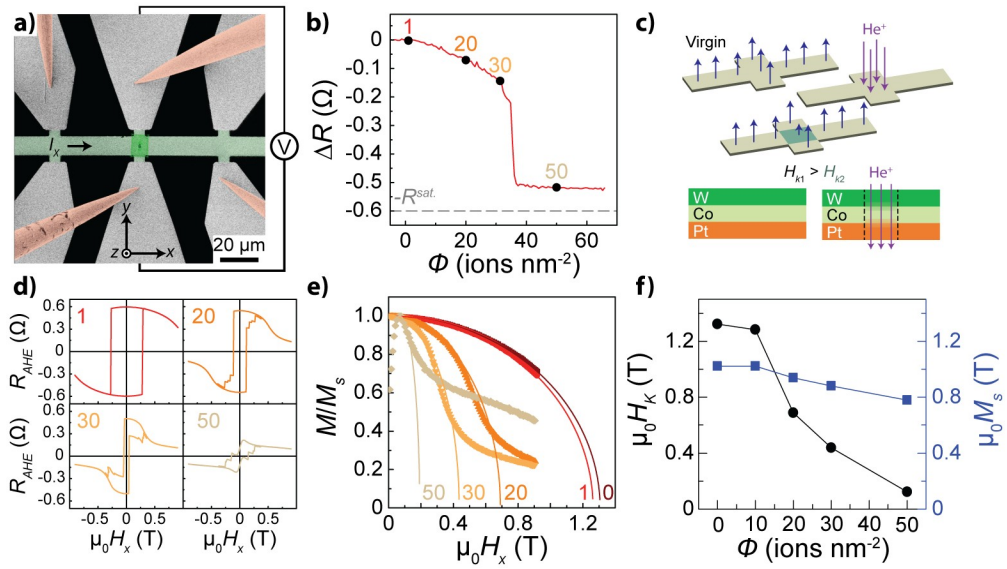

Figure 2. a) False coloured helium ion microscopy image of the *in-situ* contacting of a 10 µm Hall bar structure. The grey areas are the gold contact pads, the green stripe represents the magnetic multilayer under investigation and red denotes the needle probes. One such image corresponds to a dose of only 0.1 ions/nm². An overlay schematic shows the current and voltage lines used. **b)** *In-situ* change in anomalous Hall resistivity as a function of irradiation dose between 0 and 70 ions/nm². **c)** Schematic of the local irradiation process, whereby the local anisotropy is reduced due to interface mixing of the upper and lower Co / HM interfaces. **d)** *Ex-situ* R_{AHE} versus $\mu_0 H_x$ curves at selected doses marked in a): 1 ion/nm², 20 ions/nm², 30 ions/nm², and 50 ions/nm². **e)** Normalised magnetisation from d) for all irradiated and virgin samples, with solid line fits using eq. (1) to determine the anisotropy field, as a function of irradiation dose; **f)** Anisotropy field and saturation magnetisation determined from *ex-situ* anomalous Hall effect loops.

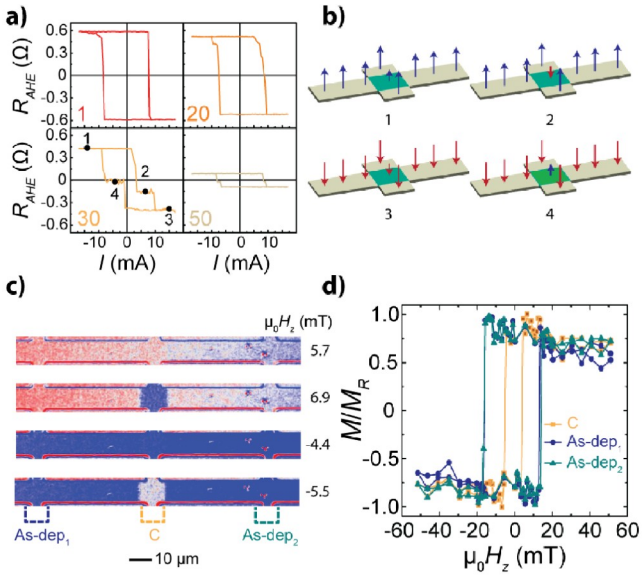

Figure 3. a) Current driven SOT switching curves at the same doses as Fig. 2 under a bias field of $\mu_0 H_x$ = 150 mT; **b)** Schematic of 4 distinct magnetic configurations achievable through electric current switching, numbered 1–4 in 30 ions nm^{-2} sub-panel of panel a); **c)** MOKE images of the Hall bar under 4 different external fields, $\mu_0 H_z$, displaying the 4 different magnetic states shown in panel b; **d)** MOKE-acquired hysteresis loops for the device receiving a dose of 30 ions nm^{-2} at three different 10 × 10 μm^2 areas: one irradiated region and two non-irradiated regions as show in panel c).

Table 1. Irradiation dose dependency of the thin film magnetic properties.

Dose	K_{eff}	Δ	$I_c^{-¿¿}$	$I_c^{+¿¿}$	$J_c^{-¿¿}$	$J_c^{+¿¿}$	J_c^{th}	η	η_i
ions nm^{-2}	kJ m^{-3}		mA	mA	MAcm^{-2}	MAcm^{-2}	MA cm^{-2}	ps	fs
0	537	133	-7.5	7.5	-6.0	6.0	459	109	15.0
1	521	129	-7.5	7.5	-6.0	6.0	442	106	15.5
20	257	64	-6.2	7.5	-5.0	6.0	184	68	31.4
30	153	39	-1.0	3.3	-0.8	2.7	85	1381	52.7
50	38	9	–	–	–	–	–	–	–

The properties are: effective anisotropy K_{eff}, thermal stability criterion Δ, negative and positive critical currents $I_c^{-¿,I_c^{+¿¿}¿}$, current densities $J_c^{-¿,J_c^{+¿¿}¿}$, the theoretical current density J_c^{th} determined using Eq. (3) with $\mu_0 H_x$ = 150 mT, and an effective spin hall angle θ_{SH}= 0.3[32,33], the switching efficiency η, determined with ρ = 9.67 μΩ.cm using eq. (4), and intrinsic efficiency η_i using eq. (5). Note that for 50 ions/nm^2, only switching of adjacent unirradiated regions was detected.

Table 2. Comparing Switching Efficiencies.

Stack	J_c [a]	B_x	Δ [b]	P [c]	η [d]	η_i	Ref.
	MA cm^{-2}	mT		PW m^{-3}	ps	fs	
Ta 3/Co 0.6/AlO_x 1.6	78	47.5	74	94	0.59	2.19	[10]
Ta 3/Pt 5/Co 0.6/Cr 2/Ta 5	2.70	20	195	0.47	106	2.30	[28]
Ta 3/Pt 5/Co 0.8/W 3/TaO_x 2	2.30	5	136	0.42	69	0.78	[34]
Ta 5/ CoFeB 1.1/ MgO 2/ Ta 2	3.09	20	56	1.91	14	0.19	[35]
Bi_2Se_3 7.4 [e]/CoTb 4.6/SiN_x 3	1.72	350	356	2.48	6.23	0.23	[36]
Pt 5/ $BaFe_{12}O_{19}$ 3 [f]	3	100	73	0.54	201	0.42	[27]

a) If $J_c^- \neq J_c^+$, then the smaller of the two values is taken; **b)** calculated for $\mu_0 H_x = 0$; **c)** when not reported, calculated using bulk resistivity values, from[37]; **d)** when not reported, literature values of θ_{SH} were taken from[38], and for multilayers with adjacent layers of opposite θ_{SH}, the magnitude of the larger one was chosen; **e)** topological insulator used for spin injection; **f)** ferromagnetic insulator.

ASSOCIATED CONTENT
Supporting Information.

The following files are available free of charge.

Supporting video 1, "MOKE_C_30ions.avi":

Ex-situ normalised magnetisation of a 10 μm wide Hall bar under a magnetic field sweep from -50 mT to +50 mT and then back to -50mT using a MOKE microscope. The central 10 x 10 μm^2 area was irradiated with a dose of 30 ions/nm^2.

Supporting text, "DEPNA_single_layer_SI.pdf":

Derivation of equation (1) using a macrospin approximation, and an example fit to sample irradiated with 20 ions nm^{-2}.

Anomalous Hall resistance plots for 8 non-irradiated samples for $\mu_0 H_z$ and $\mu_0 H_x$.

Data and Code Availability Source data for figures 1-3 and any other data that support the findings of this study, and the scripts used to process the data, are available on the Zenodo data repository: https://zenodo.org/communities/mami-h2020/

AUTHOR INFORMATION

Corresponding Authors

*peter.dunne@ipcms.unistra.fr

*c.fowley@hzdr.de

Author Contributions

The manuscript was written through contributions of all authors. All authors have given approval to the final version of the manuscript.

Funding Sources

We acknowledge the support of the Labex NIE 11-LABX-0058_NIE within the Investissement d'Avenir program ANR-10-IDEX-0002-02. This project has received funding from the European Union's Horizon 2020 research and innovation programme under the Marie Skłodowska-Curie grant agreement No 766007.

Notes

The authors declare no competing financial interest.

Acknowledgements

We thank Fabien Chevrier for technical support, the staff of the STnano nanofabrication facility. The nanofabrication facilities (NanoFaRo) at the Ion Beam Center at the HZDR are also gratefully acknowledged.

ABBREVIATIONS

HM, Heavy metal; MRAM, magnetic random-access memory; PMA, perpendicular magnetic anisotropy; SOT, spin orbit torque

REFERENCES

(1) Baibich, M. N.; Broto, J. M.; Fert, A.; Van Dau, F. N.; Petroff, F.; Etienne, P.; Creuzet, G.; Friederich, A.; Chazelas, J. Giant Magnetoresistance of (001)Fe/(001)Cr Magnetic Superlattices. *Phys. Rev. Lett.* **1988**, *61* (21), 2472–2475. https://doi.org/10.1103/PhysRevLett.61.2472.

(2) Binasch, G.; Grünberg, P.; Saurenbach, F.; Zinn, W. Enhanced Magnetoresistance in Layered Magnetic Structures with Antiferromagnetic Interlayer Exchange. *Phys. Rev. B* **1989**, *39* (7), 4828–4830. https://doi.org/10.1103/PhysRevB.39.4828.

(3) Slonczewski, J. C. Current-Driven Excitation of Magnetic Multilayers. *J. Magn. Magn. Mater.* **1996**, *159* (1), L1–L7. https://doi.org/10.1016/0304-8853(96)00062-5.

(4) Myers, E. B.; Ralph, D. C.; Katine, J. A.; Louie, R. N.; Buhrman, R. A. Current-Induced Switching of Domains in Magnetic Multilayer Devices. *Science* **1999**, *285* (5429), 867–870. https://doi.org/10.1126/science.285.5429.867.
(5) Kiselev, S. I.; Sankey, J. C.; Krivorotov, I. N.; Emley, N. C.; Schoelkopf, R. J.; Buhrman, R. A.; Ralph, D. C. Microwave Oscillations of a Nanomagnet Driven by a Spin-Polarized Current. *Nature* **2003**, *425* (6956), 380–383. https://doi.org/10.1038/nature01967.
(6) IBM Unveils 19TB SSD With Everspin MRAM Data Cache | Everspin https://www.everspin.com/news/ibm-unveils-19tb-ssd-everspin-mram-data-cache (accessed Nov 19, 2019).
(7) Miron, I. M.; Garello, K.; Gaudin, G.; Zermatten, P.-J.; Costache, M. V.; Auffret, S.; Bandiera, S.; Rodmacq, B.; Schuhl, A.; Gambardella, P. Perpendicular Switching of a Single Ferromagnetic Layer Induced by In-Plane Current Injection. *Nature* **2011**, *476* (7359), 189. https://doi.org/10.1038/nature10309.
(8) Gambardella, P.; Miron, I. M. Current-Induced Spin–Orbit Torques. *Philos. Trans. R. Soc. Lond. Math. Phys. Eng. Sci.* **2011**, *369* (1948), 3175–3197. https://doi.org/10.1098/rsta.2010.0336.
(9) Liu, L.; Pai, C.-F.; Li, Y.; Tseng, H. W.; Ralph, D. C.; Buhrman, R. A. Spin-Torque Switching with the Giant Spin Hall Effect of Tantalum. *Science* **2012**, *336* (6081), 555–558. https://doi.org/10.1126/science.1218197.
(10) Miron, I. M.; Gaudin, G.; Auffret, S.; Rodmacq, B.; Schuhl, A.; Pizzini, S.; Vogel, J.; Gambardella, P. Current-Driven Spin Torque Induced by the Rashba Effect in a Ferromagnetic Metal Layer. *Nat. Mater.* **2010**, *9* (3), 230. https://doi.org/10.1038/nmat2613.
(11) Perrissin, N.; Lequeux, S.; Strelkov, N.; Chavent, A.; Vila, L.; Buda-Prejbeanu, L. D.; Auffret, S.; Sousa, R. C.; Prejbeanu, I. L.; Dieny, B. A Highly Thermally Stable Sub-20 Nm Magnetic Random-Access Memory Based on Perpendicular Shape Anisotropy. *Nanoscale* **2018**, *10* (25), 12187–12195. https://doi.org/10.1039/C8NR01365A.
(12) Wagner, K.; Kákay, A.; Schultheiss, K.; Henschke, A.; Sebastian, T.; Schultheiss, H. Magnetic Domain Walls as Reconfigurable Spin-Wave Nanochannels. *Nat. Nanotechnol.* **2016**, *11* (5), 432–436. https://doi.org/10.1038/nnano.2015.339.
(13) Fassbender, J.; Ravelosona, D.; Samson, Y. Tailoring Magnetism by Light-Ion Irradiation. *J. Phys. Appl. Phys.* **2004**, *37* (16), R179–R196. https://doi.org/10.1088/0022-3727/37/16/R01.
(14) Hoshi, Y.; Naoe, M. Differences between Sputtering Methods in The Formation of Amorphous Magnetic Alloy Films. *MRS Online Proc. Libr. Arch.* **1985**, *58*. https://doi.org/10.1557/PROC-58-75.
(15) Chappert, C.; Bernas, H.; Ferré, J.; Kottler, V.; Jamet, J.-P.; Chen, Y.; Cambril, E.; Devolder, T.; Rousseaux, F.; Mathet, V.; Launois, H. Planar Patterned Magnetic Media Obtained by Ion Irradiation. *Science* **1998**, *280* (5371), 1919–1922. https://doi.org/10.1126/science.280.5371.1919.
(16) Zhao, X.; Zhang, B.; Vernier, N.; Zhang, X.; Sall, M.; Xing, T.; Diez, L. H.; Hepburn, C.; Wang, L.; Durin, G.; Casiraghi, A.; Belmeguenai, M.; Roussigné, Y.; Stashkevich, A.; Chérif, S. M.; Langer, J.; Ocker, B.; Jaiswal, S.; Jakob, G.; Kläui, M.; Zhao, W.; Ravelosona, D. Enhancing Domain Wall Velocity through Interface Intermixing in W-CoFeB-MgO Films with Perpendicular Anisotropy. *Appl. Phys. Lett.* **2019**, *115* (12), 122404. https://doi.org/10.1063/1.5121357.

(17) Jiang, S.; Khymyn, R.; Chung, S.; Le, T. Q.; Diez, L. H.; Houshang, A.; Zahedinejad, M.; Ravelosona, D.; Åkerman, J. Reduced Spin Torque Nano-Oscillator Linewidth Using He + Irradiation. *Appl. Phys. Lett.* **2020**, *116* (7), 072403. https://doi.org/10.1063/1.5137837.
(18) Yun, J.; Zuo, Y.; Mao, J.; Chang, M.; Zhang, S.; Liu, J.; Xi, L. Lowering Critical Current Density for Spin-Orbit Torque Induced Magnetization Switching by Ion Irradiation. *Appl. Phys. Lett.* **2019**, *115* (3), 032404. https://doi.org/10.1063/1.5111937.
(19) Franken, J. H.; Hoeijmakers, M.; Lavrijsen, R.; Kohlhepp, J. T.; Swagten, H. J. M.; Koopmans, B.; van Veldhoven, E.; Maas, D. J. Precise Control of Domain Wall Injection and Pinning Using Helium and Gallium Focused Ion Beams. *J. Appl. Phys.* **2011**, *109* (7), 07D504. https://doi.org/10.1063/1.3549589.
(20) Fowley, C.; Diao, Z.; Faulkner, C. C.; Kally, J.; Ackland, K.; Behan, G.; Zhang, H. Z.; Deac, A. M.; Coey, J. M. D. Local Modification of Magnetic Anisotropy and Ion Milling of Co/Pt Multilayers Using a He + Ion Beam Microscope. *J. Phys. Appl. Phys.* **2013**, *46* (19), 195501. https://doi.org/10.1088/0022-3727/46/19/195501.
(21) Röder, F.; Hlawacek, G.; Wintz, S.; Hübner, R.; Bischoff, L.; Lichte, H.; Potzger, K.; Lindner, J.; Fassbender, J.; Bali, R. Direct Depth- and Lateral- Imaging of Nanoscale Magnets Generated by Ion Impact. *Sci. Rep.* **2015**, *5*, 16786. https://doi.org/10.1038/srep16786.
(22) Hlawacek, G.; Veligura, V.; van Gastel, R.; Poelsema, B. Helium Ion Microscopy. *J. Vac. Sci. Technol. B* **2014**, *32* (2), 020801. https://doi.org/10.1116/1.4863676.
(23) Woo, S.; Mann, M.; Tan, A. J.; Caretta, L.; Beach, G. S. D. Enhanced Spin-Orbit Torques in Pt/Co/Ta Heterostructures. *Appl. Phys. Lett.* **2014**, *105* (21), 212404. https://doi.org/10.1063/1.4902529.
(24) Carcia, P. F. Perpendicular Magnetic Anisotropy in Pd/Co and Pt/Co Thin-film Layered Structures. *J. Appl. Phys.* **1988**, *63* (10), 5066–5073. https://doi.org/10.1063/1.340404.
(25) Fowley, C.; Ouardi, S.; Kubota, T.; Yildirim, O.; Neudert, A.; Lenz, K.; Sluka, V.; Lindner, J.; Law, J. M.; Mizukami, S.; Fecher, G. H.; Felser, C.; Deac, A. M. Direct Measurement of the Magnetic Anisotropy Field in Mn–Ga and Mn–Co–Ga Heusler Films. *J. Phys. Appl. Phys.* **2015**, *48* (16), 164006. https://doi.org/10.1088/0022-3727/48/16/164006.
(26) Lee, K.-S.; Lee, S.-W.; Min, B.-C.; Lee, K.-J. Threshold Current for Switching of a Perpendicular Magnetic Layer Induced by Spin Hall Effect. *Appl. Phys. Lett.* **2013**, *102* (11), 112410. https://doi.org/10.1063/1.4798288.
(27) Li, P.; Liu, T.; Chang, H.; Kalitsov, A.; Zhang, W.; Csaba, G.; Li, W.; Richardson, D.; DeMann, A.; Rimal, G.; Dey, H.; Jiang, J. S.; Porod, W.; Field, S. B.; Tang, J.; Marconi, M. C.; Hoffmann, A.; Mryasov, O.; Wu, M. Spin–Orbit Torque-Assisted Switching in Magnetic Insulator Thin Films with Perpendicular Magnetic Anisotropy. *Nat. Commun.* **2016**, *7*, 12688. https://doi.org/10.1038/ncomms12688.
(28) Cui, B.; Li, D.; Yun, J.; Zuo, Y.; Guo, X.; Wu, K.; Zhang, X.; Wang, Y.; Xi, L.; Xue, D. Magnetization Switching through Domain Wall Motion in Pt/Co/Cr Racetracks with the Assistance of the Accompanying Joule Heating Effect. *Phys. Chem. Chem. Phys.* **2018**, *20* (15), 9904–9909. https://doi.org/10.1039/C7CP08352A.
(29) Evans, R. F. L.; Chantrell, R. W.; Nowak, U.; Lyberatos, A.; Richter, H.-J. Thermally Induced Error: Density Limit for Magnetic Data Storage. *Appl. Phys. Lett.* **2012**, *100* (10), 102402. https://doi.org/10.1063/1.3691196.
(30) Weller, D.; Moser, A. Thermal Effect Limits in Ultrahigh-Density Magnetic Recording. *IEEE Trans. Magn.* **1999**, *35* (6), 4423–4439. https://doi.org/10.1109/20.809134.

(31) Fulara, H.; Zahedinejad, M.; Khymyn, R.; Awad, A. A.; Muralidhar, S.; Dvornik, M.; Åkerman, J. Spin-Orbit Torque–Driven Propagating Spin Waves. *Sci. Adv.* **2019**, *5* (9), eaax8467. https://doi.org/10.1126/sciadv.aax8467.
(32) Pai, C.-F.; Liu, L.; Li, Y.; Tseng, H. W.; Ralph, D. C.; Buhrman, R. A. Spin Transfer Torque Devices Utilizing the Giant Spin Hall Effect of Tungsten. *Appl. Phys. Lett.* **2012**, *101* (12), 122404. https://doi.org/10.1063/1.4753947.
(33) Hao, Q.; Chen, W.; Xiao, G. Beta (β) Tungsten Thin Films: Structure, Electron Transport, and Giant Spin Hall Effect. *Appl. Phys. Lett.* **2015**, *106* (18), 182403. https://doi.org/10.1063/1.4919867.
(34) Zhang, X.; Mao, J.; Chang, M.; Yan, Z.; Zuo, Y.; Xi, L. Current-Induced Magnetization Switching in Pt/Co/W and Pt/Co/$W_{0.82}Pt_{0.18}$ Structures with Perpendicular Magnetic Anisotropy. *J. Phys. Appl. Phys.* **2020**. https://doi.org/10.1088/1361-6463/ab7c9b.
(35) Li, S. K.; Zhao, X. T.; Liu, W.; Song, Y. H.; Liu, L.; Zhao, X. G.; Zhang, Z. D. Interface Effect of Ultrathin W Layer on Spin-Orbit Torque in Ta/W/CoFeB Multilayers. *Appl. Phys. Lett.* **2019**, *114* (8), 082402. https://doi.org/10.1063/1.5081965.
(36) Han, J.; Richardella, A.; Siddiqui, S. A.; Finley, J.; Samarth, N.; Liu, L. Room-Temperature Spin-Orbit Torque Switching Induced by a Topological Insulator. *Phys. Rev. Lett.* **2017**, *119* (7), 077702. https://doi.org/10.1103/PhysRevLett.119.077702.
(37) Haynes, W. M. *CRC Handbook of Chemistry and Physics*; CRC Press, 2016.
(38) Sinova, J.; Valenzuela, S. O.; Wunderlich, J.; Back, C. H.; Jungwirth, T. Spin Hall Effects. *Rev. Mod. Phys.* **2015**, *87* (4), 1213–1260. https://doi.org/10.1103/RevModPhys.87.1213.

For Table of Contents Only: